Indian Journal of Pure & Applied Physics
Vol. 59, September 2021, pp. 612-618

Copper Nanowire Arrays: Growth and Properties

Bharti Sharma[a,c], Ram Mehar Singh[a], Avshish Kumar[b] & Sushil Kumar[a*]

[a]Department of Physics, Chaudhary Devi Lal University, Sirsa, 125 055, Haryana India

[b]Amity Institute for Advanced Research and Studies (Materials & Devices), Amity University, Noida, 201 313, Uttar Pradesh, India

[c]Department of Physics, Government National College, Sirsa, 125 055, Haryana, India

Received 9 June 2021; accepted 5 July 2021

Cu nanowire arrays of three different diameters have been synthesized via template assisted electrode position technique. Morphological, structural, optical, electrical and field emission properties were examined for these three nanowire arrays. Morphological study reveals the nanowire arrays are of uniform diameter throughout the length and of desired dimensions. Structural study shows the face centred cubic structure of nanowires. The crystallite size has been calculated using the Debye-Scherrer relation and micro strain has been calculated using Williamson-Hall analysis. The surface plasmon resonance absorption peak shifts towards red end with increase in diameter of nanowires. I-V characteristics show the ohmic behaviour. Electron field emission properties of Cu nanowire arrays have been studied using Fowler Nordheim theory. The field emission parameters like maximum emission current density, turn on field and field enhancement factor have been calculated for nanowire arrays of different diameters. Cu nanowire arrays of diameter 50 nm exhibit better field emission properties, indicating that thin nanowire arrays have great potential to be used as field emitters.

Keywords: Nanowires, Electrodeposition, Surface plasmon resonance, Electrical Conductivity, Field emitters

1 Introduction

One dimensional nanostructures especially nanowires, have gained huge attention on account of their fascinating and unexpected properties, compared to that of bulk counterparts[1].Nanowires made of copper have been widely studied on account of its high electrical conductivity, large abundance and low cost in comparison to that of silver and gold[2-4]. Cu nanowires have numerous applications which encompasses electron emitters, metallic interconnect, sensor, and field emission displays[5-8]. Among the numerous methods to fabricate the nanowires, template based electrode position is an easy, precise and low cost technique. Template synthesis using track etched polycarbonate membrane as template has become a popular method to fabricate the nanowires[9-11]. In template based synthesis, morphology of fabricated nanowire arrays rely absolutely on the shape and size of pores of the template[12-14]. The factors like morphology, length, diameter and density of nanowires play a versatile role on the properties of nanowires desirable for device fabrication[15].

Several studies have investigated the size effect on the properties of nanowires. Narula *et al*. studied the variation in the structural, optical and electrical properties of CdSe nanowires with diameter[16]. Duan *et al*. and Locharoenrat *et al*. had studied optical properties of Cu nanowires and observed that with increasing diameter and increasing length of wire, surface plasmon resonance absorption peak is red shifted[17, 18]. Qian *et al*. had studied the effect of aspect ratio of Zn Onanorod arrays on their field emission behaviour[19]. The work done so far to investigate the impact of diameter on the electrical and field emission behaviour of Cu nanowire arrays is minimal and needs to be enriched.

Here, authors have prepared Cu nanowires of three different diameters using template assisted electrode position technique and elaborated the employed fabrication technique and characterization methods. The results related to morphology, structural, optical, electrical and field emission studies have been discussed. There is noticeable change in the properties of the nanowires with diameter and authors have sincerely attempted to explain the same. The present study is significant as the properties of Cu nanowires can be tuned by altering aspect ratio for their employability as nanoconnectors and in nanoscale devices.

2 Experimental work

2.1 Preparation of copper nanowire arrays

Commercially available track-etched polycarbonate membranes (Whatman) of 10μm thickness, quoted

*Corresponding author: (Email: sushil_phys@rediffmail.com)

pore diameter of 100, 80 and 50nm and pore density of 10^6 cm^{-2} were utilized as templates for the synthesis of nanowire arrays. All the chemical reagents used in synthesis were of high purity and of analytical grade. Deionized water was used for the preparation of the solutions. The polycarbonate membrane is preferably used in template synthesis because it can be easily removed via dissolution in dichloromethane to get the desired nanowire arrays.

Two electrode cell[20] made of perspex, consisting of template on Cu substrate as working electrode (cathode) and copper rod as counter electrode (anode), was used for electrode position of copper in the pores of the template in order to fabricate Cu nanowire arrays. The aqueous solution containing 0.4M $CuSO_4.5H_2O$ with pH value 1.8-2.0 was used as electrolyte. Sulphuric acid (H_2SO_4) was employed to maintain the suitable pH of solution. The electrode position proceeded at a fixed potential of 0.5 V at room temperature for 10 min. Three samples of Cu nanowire arrays with different pore diameters 100, 80 and 50 nm have been fabricated successfully within the tracketched membranes.

2.2 Characterization methods

Morphology of synthesized nanowires was investigated by field emission scanning electron microscopy (FESEM) using Hitachi UHR FESEM SU8010. The elemental composition was obtained by energy dispersive X-ray spectres copy (EDX) using a system attached with FESEM. The crystallographic information was received from X-ray diffractometer (RigakuMini-Flex II) with CuKα (1.5406 Å) radiation in the scanning range 2θ ~ 10-80°. Optical properties have been determined with UV-visible spectro-photometer (ShimadzuUV-1650 PC). I-V characteristics of Cu nanowire arrays were measured with Keithley 2400 source meter. Field emission characterization was performed at room temperature in a specially designed sample chamber having vacuum of the order of 10^{-6} mbar.

3 Results and discussion

3.1 Morphological study and elemental analysis

The morphology of the fabricated nanowires has been studied using FESEM after the dissolution of the polycarbonate membrane in the dichloromethane. It can be seen from the images shown in Fig. 1 that the

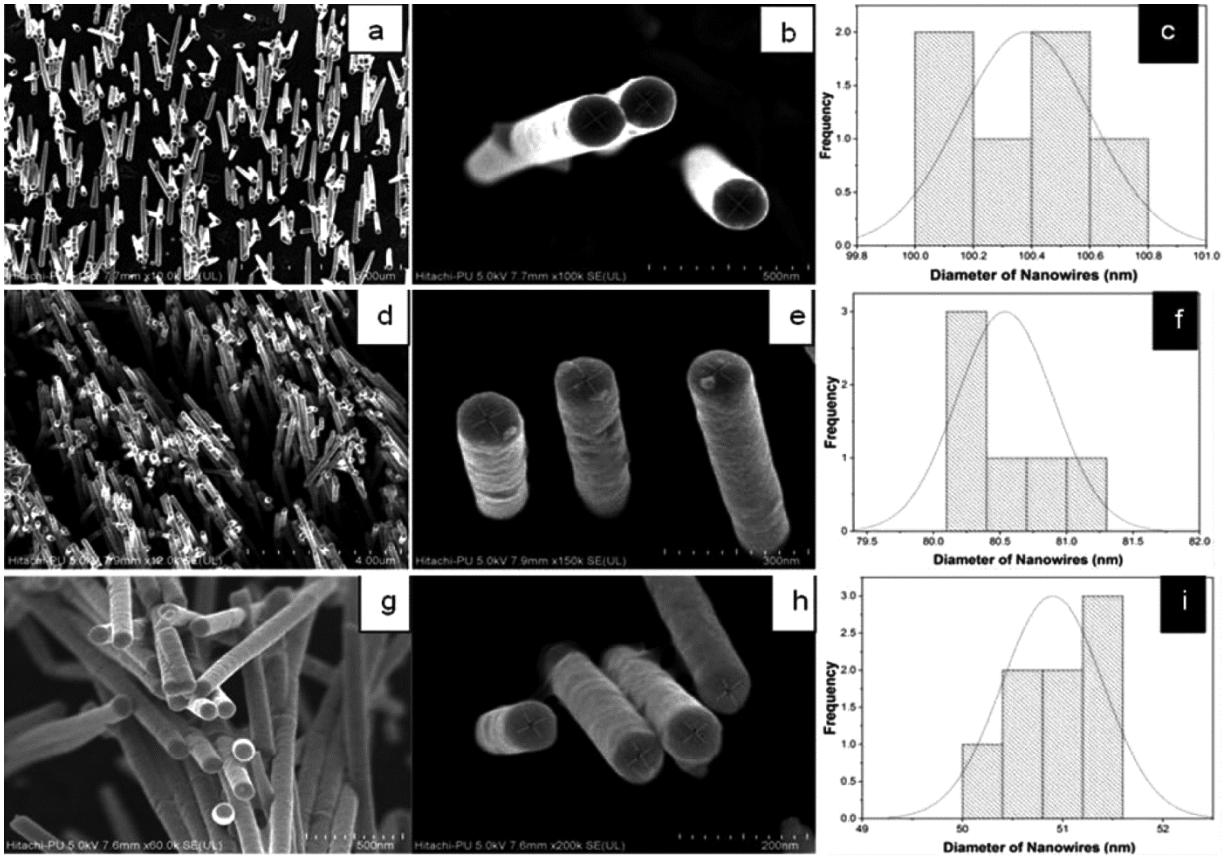

Fig. 1— FESEM images of Cu nanowires at different magnifications and histograms showing diameters of Cu nanowires: (a-c) 100 nm, (d-f) 80 nm and (g-i) 50 nm.

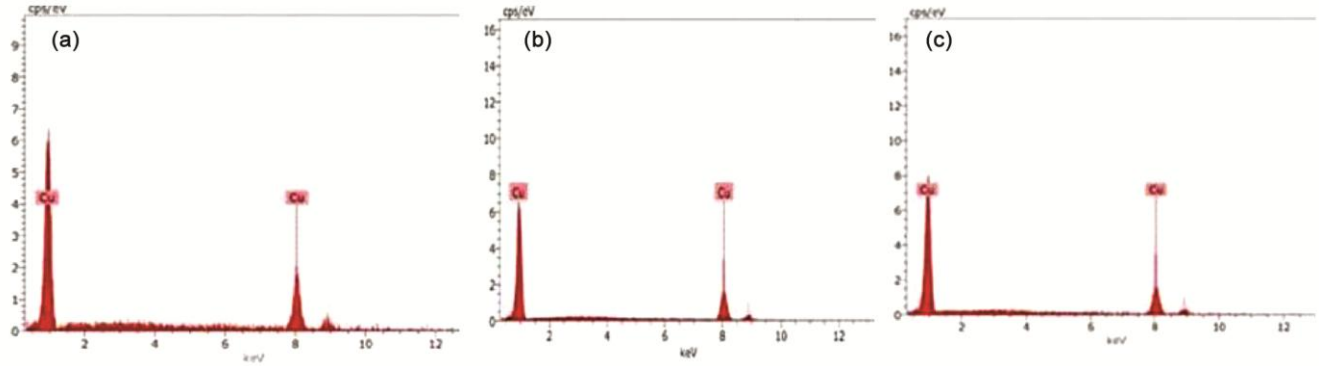

Fig. 2 — EDX spectra of Cu nanowires of different diameters: (a) 100 nm, (b) 80 nm and (c) 50 nm.

synthesized nanowires are smooth, dense and uniform in diameter. Some nanowires are slightly tilted which could have happened during the process of dissolution. The diameter of nanowires has been calculated using Image J software and is almost same as that of the pore diameter (*i.e*. 100, 80 and 50 nm) of template used. The length of nanowires is almost equal to the thickness of the template *i.e.*10 μm.

The fabrication of copper nanowires is based on the reduction of Cu^{2+} ions in to Cu when potential difference is applied across the working electrode and the counter electrode. After the generation of grains of copper at the bottom of pores of the template, the nanowires start growing vertically upward along the pore length, as a result of trapping effect of pores[21].In EDX spectra of copper nanowires, as shown in Fig. 2 , all the three peaks are of copper[22, 23]. It confirmed that the fabricated nanowires are of pure copper without any signature of oxidation.

3.2Structural analysis

X-ray diffraction (XRD) patterns obtained for the Cu nanowires embedded in polycarbonate membrane of diameters 100, 80 and 50 nm are shown in Fig. 3. There are clearly noticeable three peaks which can be indexed to face centred cubic structure[24].The three peaks positioned at 43.36^0, 50.5^0 and 74.21° correspond to (111), (200) and (220) crystal planes respectively [JCPDS card no - 04-0836]. There is no peak from polycarbonate membrane due to its amorphous nature. The sharp intense peaks points towards good crystallinity of nanowires. It has been observed that, with decrease in the diameter of the nanowires, there is no peak shift as well as no change in growth orientation of nanowires. This shows that aspect ratio does not influence the lattice structure of nanowires. Nevertheless, there is slight decrease in the width and intensity of the peaks with the decrease

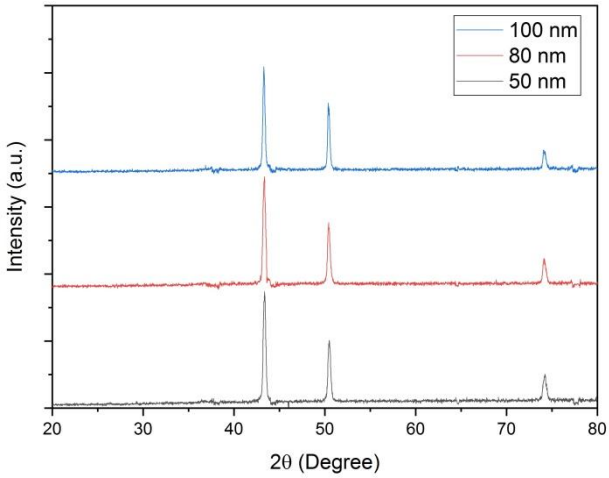

Fig. 3 — XRD pattern obtained for Cu nanowires of different diameters.

in diameter. The estimated value of lattice constant, a=3.61 Å is same for all the nanowires with different diameters and agrees well with the reported value[25]. The various structural parameters *i.e.* crystallite size, degree of crystallinity, microstrain and dislocation density have also been calculated as follows:

The crystallite size has been calculated using Debye Scherrer relation[26] and is given by:

$$D = \frac{k\lambda}{\beta \cos\theta} \quad \ldots (1)$$

where k (= 0.9) is a shape factor, λ (= 0.15406 nm) is the wavelength of CuKα line, θ is the Bragg angle and β is the peak width at half maximum (in radian). The average value of crystallite size is 29.04, 27.34 and 26.03 nm for Cu nanowires of diameter 100, 80 and 50 nm respectively. There is decrease in the crystallite size with decrease in size. The dislocation density (δ) which gives the information about the deformations in the crystal and is a measure of number of dislocations per unit volume in a material.

It can be calculated using the relation $\delta = 1/D^2$ and found to be 1.18 x 10^{-3}, 1.33 x 10^{-3} and 1.48 x 10^{-3} for diameter 100, 80 and 50 nm respectively. Williamson-Hall (WH) method[27] has been used to study the microstructure of the lattice *i.e.* intrinsic microstrain and to provide the average crystallite size. The presence of microstrain in the nanocrystal is because of grain boundaries and surface defects due to reduction in size and can be calculated using the relation. The broadening of peak in XRD pattern is due to the combined effect of size and strain of the nanowire. The broadening due to size is given by eq. (1) and the broadening due to strain is 4ε tanθ where ε is microstrain. Thus, total broadening is given by:

$$\beta_T \cos\theta = \varepsilon\,(4\sin\theta) + \frac{k\lambda}{D} \quad \ldots (2)$$

Eq. (2) depicts the straight line equation in which ε denotes the slope and kλ/D denotes the intercept. The graph was plotted taking 4 sinθ on X-axis and β_T cosθ on Y-axis, and fitted linearly, as shown in Fig. 4. The value of microstrain has been determined from the slope, found to be 1.14 x 10^{-3}, 1.32 x 10^{-3} and 1.54 x 10^{-3} for Cu nanowires of diameter 100, 80 and 50 nm respectively. It has been observed that there is decrease in crystallite size and increase in microstrain with decrease in diameter which is due to the size effect.

3.3 Optical study

The optical properties of prepared copper nanowires have been studied using UV-visible absorption spectra as depicted in Fig. 5.The spectra revealed the absorption peak in the visible region at 576, 570 and 562 nm in case of Cu nanowires of diameter 100, 80 and 50 nm respectively. When the size is reduced to the nanoscale, absorption peak in the visible region appears owing to surface plasmon resonance (SPR). This absorption peak does not present in bulk copper.SPR in the metallic nanoparticles is the result of oscillations of the conduction electrons with respect to the heavy core of nanoparticles induced by the electromagnetic field[1]. The position and width of surface plasmon absorption peak depends upon the dimensions and composition of nanowires. It is observed that absorption peak shifts to lower wavelength with decrease in the diameter of the nanowire. This blue shift is because of the enhanced electron surface scattering with decrease in the diameter, as the electrons can reach the surface faster and got scattered quickly. The literature[17, 18,28] has also suggested the same.

3.4 Electrical behaviour

I-V characteristics of Cu nanowires were recorded, as shown in Fig. 6, for three different diameters using two electrode cell and Keithley 2400 source meter. The copper substrate acts as one electrode and the tungsten tip as other electrode. The curve comes out to be linear for all the three nanowire arrays with different diameters showing the ohmic behaviour. The slope of the curve directly indicates the value of ohmic resistance i.e. 0.73, 0.79 and 0.84 Ω for nanowires of diameter 100, 80 and 50 nm respectively. The calculated value of resistance was meant for the bundle of nanowires that were in contact with the tungsten tip. The electrical conductivity (σ) for nanowires obey the relation given below since the length of nanowire is larger than the mean free path of electron:

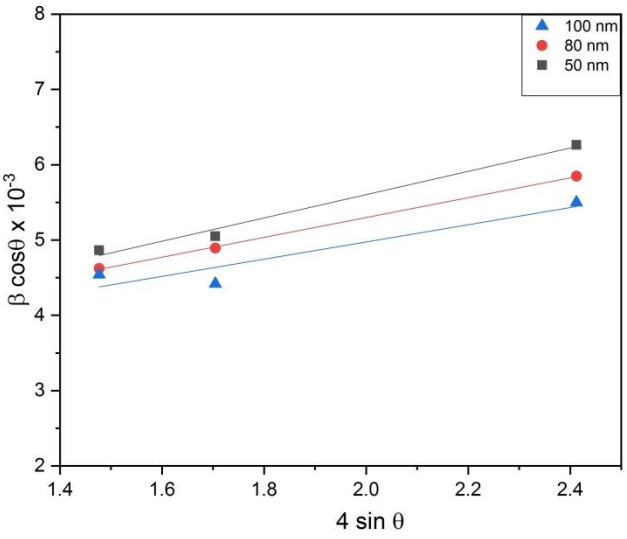

Fig. 4— W-H plot for Cu nanowires of different diameters.

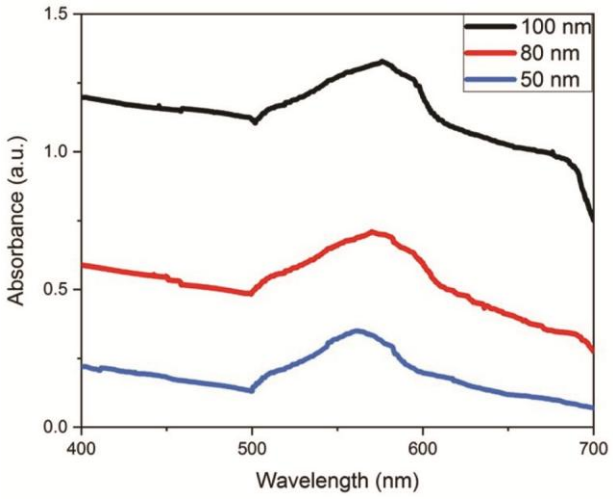

Fig. 5 — Absorption spectra of Cu nanowires of different diameters

$$\sigma = \frac{dI}{dV} * \frac{l}{A} \quad \text{... (3)}$$

where l is length of nanowires (here, equal to 10 μm), A is the cross sectional area in contact which is same as the area of tungsten tip and dI/dV is slope of I-V curve. Here, l/A is same for nanowires of all three diameters. Therefore, the value of conductivity is directly proportional to the slope. Thus, we can say that electrical conductivity decreases with decrease in the diameter of nanowire. This is due to the fact that when the size is reduced to nanoscale there is increase in grain boundary scattering and surface scattering [16, 29-31].

3.5 Field emission behaviour

Field emission behaviour was analysed using the cathode-anode arrangement in a specially designed sample chamber as shown in Fig. 7. The tip of vertically aligned Cu nanowire arrays act as electron emitters. The ends of nanowires stuck on Cu tape acts as cathode and the conical stainless steel plate with area 0.785 cm^2 acts as anode. The distance between cathode and anode was maintained at 500 μm. In the present study, Cu nanowire arrays of three different diameters (100, 80 and 50 nm) were studied for field emission behaviour. From the JE curve shown in Fig. 8, authors observed the turn on field of 4.0, 3.5 and 2.5 V/μm and maximum current densities of 160, 250 and 900 μA/cm^2 respectively, for Cu nanowire arrays of diameter 100, 80 and 50 nm respectively. From these results, it may be concluded that the current density increases and turn on field decreases with reduction in diameter of grown Cu nanowires.

Theoretically, Fowler-Nordheim (F-N) theory[33-34] is being used to explain the field emission properties of various nanostructures such as carbon nanostructures, metal nanowires and metal oxide nanostructures. As per F-N theory, the emission current density (J) of nanowires, as a function of applied electric field (E) and work function (∅), can be estimated as:

$$J = \frac{A\beta^2 E^2}{\emptyset} \exp\left(\frac{-B\emptyset^{\frac{3}{2}}}{\beta E}\right) \quad \text{... (4)}$$

Here, A and B are constants having values 1.56 x10^{-6}AeVV^{-2} and 6.83 x10^7 eV$^{-3/2}$Vcm^{-1} respectively. E is the applied electric field and can be defined as βV/d, where V is the voltage between anode and cathode, d is the distance between these two electrodes, and β is the field enhancement factor. Eq. (5) shows that current density is inversely proportional to work function of the emitting nanowire. Therefore, the fabrication of nanostructures having smaller work function played vital role in field emission devices, in comparison to conventional field emitters *e.g.* silicon, diamond and molybdenum[35]. Figure 9 shows the corresponding FN

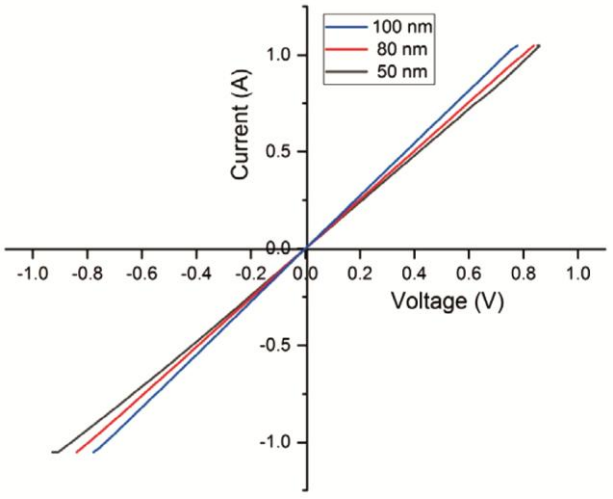

Fig. 6 — I-V characteristics of Cu nanowires of different diameters.

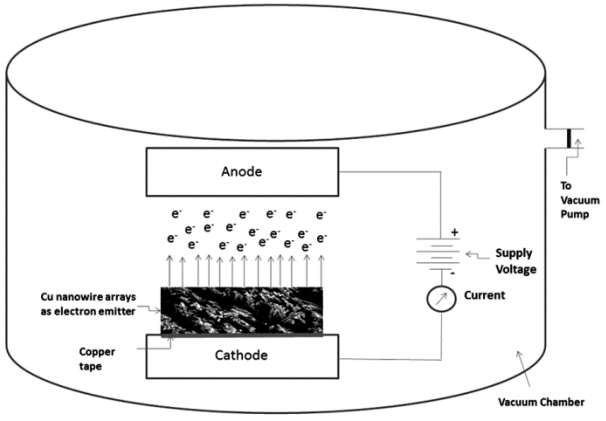

Fig. 7 — Schematic diagram of field emission measurement set up.

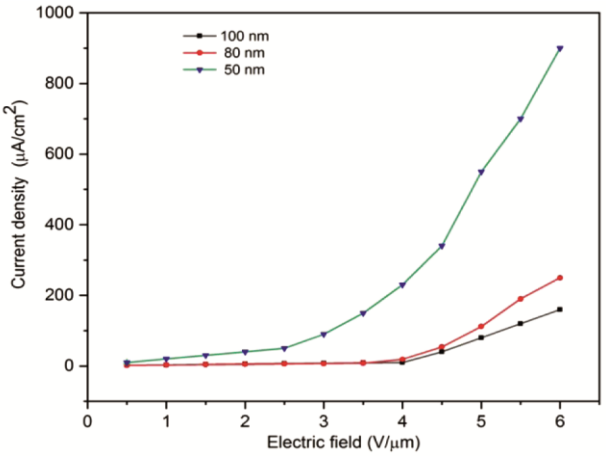

Fig. 8 — JE Curve of Cu nanowire arrays of different diameters.

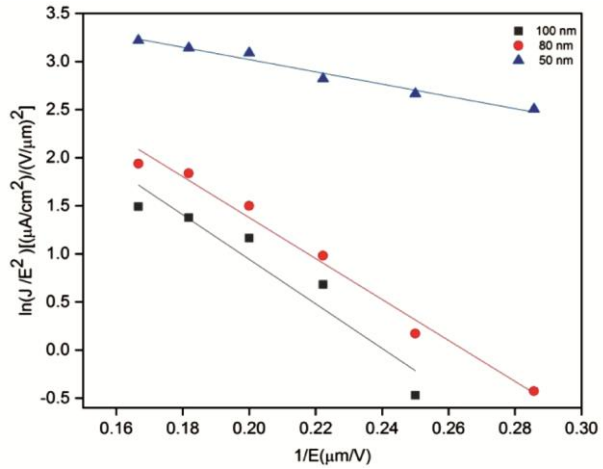

Fig. 9— FN plot of Cu nanowire arrays of different diameters.

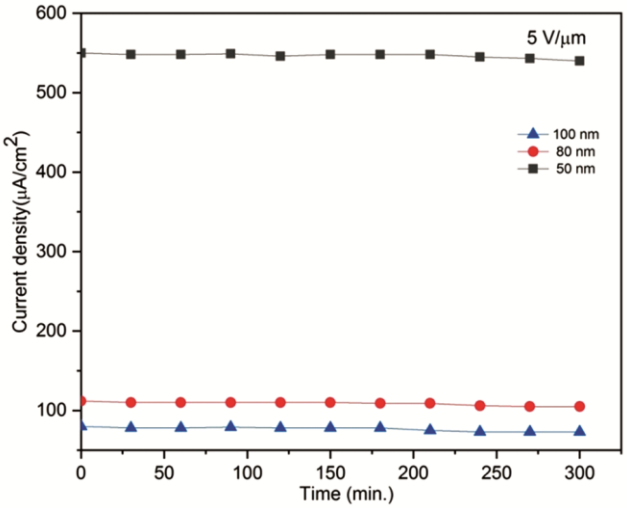

Fig. 10 — Field emission current stability curve of Cu nanowire arrays at 5V/μm.

plot ($\ln(J/E^2)$ *vs* 1/E) for all three Cu nanowire arrays. The field enhancement factor (β) can be measured from the slope (m) of FN plot as follows:

$$\beta = \frac{B\emptyset^{\frac{3}{2}}d}{m} \quad \ldots (5)$$

Here, the value of the work function used to calculate the field enhancement factor is taken as 4.5 eV. The value of β was calculated using the above eq. 6 and estimated to be 0.28 x 10^4, 0.32 x $10^4$and 1.02 x 10^4 for Cu nanowire arrays of diameter 100, 80 and 50nm respectively. Therefore, from these studies, it may be concluded that the field enhancement factor is increased as the diameter of Cu nanowire arrays is decreased. This is due to the fact that the field enhancement factor is directly proportional to the aspect ratio (length/diameter) of nanowires[19]. When the diameter of nanowires is reduced, the space between nanowires increases, resulting in reduction of field shielding effects, and because of this, the value of field enhancement factor is enhanced. The results of all three prepared nanowire arrays have been summarized in Table 1. A detailed comparison among them showed a significant improvement in field emission properties as decrease the diameter of nanowires decreases. The enhancement in all parameters of Cu nanowire arrays of diameter 50 nm can also be attributed to the higher degree of crystallinity and the removal of defects. To check the accuracy of results, the field emission study has been repeated three times under the same experimental conditions. The stability of Cu nanowire arrays as field emitters in the same experimental set up have also been studied. The variation in the field emission current density for 5 h (J-T Plot) at fixed electric field 5.0 V/μm has been noted for all three samples of Cu nanowire arrays. The J-T Plot is shown in Fig. 10 and reveals that the emission current density is almost uniform within the period of 5h in case of all samples.

Table 1 — Field emission parameters of Cu nanowire arrays of different diameters.

Diameter of Cu nanowires (nm)	Maximum Current density J (μA/cm^2)	Turn on field E (V/μm)	Field enhancement factor β
100	160	4.0	0.28 x 10^4
80	250	3.5	0.32 x 10^4
50	900	2.5	1.02 x 10^4

4 Conclusion

The arrays of Cu nanowires with different diameters were fabricated successfully using template assisted electrodeposition technique. Nanowires are densely populated and possess the diameter and length equal to the diameter and the thickness of respective templates. The results showed that the dimensions of nanowires played key role in the properties desirable for device fabrication. XRD pattern confirmed the face centred cubic structure of prepared nanowires. The surface plasmon absorption peak shifts to higher wavelength with increase in diameter of nanowires. I-V characteristics showed the ohmic behaviour of copper nanowires. The field enhancement factor β increases with decrease in the diameter of nanowires. The nanowire arrays of 50 nm diameter exhibited the best field emission properties among all three with maximum emission current density 900 μA/cm^2, turn on field 2.5 V/μm and field

enhancement factor 1.02 x 10^4. These results highlighted that electrochemically synthesized Cu nanowire arrays of reduced diameter can be a promising candidate for their applications in nanoelectronics especially as cold cathode field emitters.

Acknowledgement

Authors thank the Sophisticated Analytical Instrumentation Facility (SAIF) Panjab University, Chandigarh for FESEM, National Institute of Technology Kurukshetra for XRD, and Jamia Millia Islamia (A Central University) New Delhi for field emission facilities.

References

1 Cao G, Nanostructures & Nanomaterials: Synthesis Properties & Applications (Imperial College Press, London), 2nd Edn, 2004.
2 Li X, Wang Y, Yin C & Yin Z, *J Mater Chem C*, 8 (2002) 849.
3 Nam V B & Lee D, *Nanomaterials*, 6 (2016) 47.
4 Sharma B, Kumar S, Dixit R M & Kumar N, *AIP Conf Proc*, 2276 (2020) 020005.
5 Xavier S, Mátéfi-Tempfli S, Ferain E, Purcell S, Enouz-Védrenne S, Gangloff L, Minoux E, Hudanski L, Vincent P & Schnell J P, *Nanotechnology*, 19 (2008) 21560.
6 Zhou J, Xu N S, Deng S Z, Chen J, She J C & Wang Z L, *Adv Mater*, 15 (2003) 1835.
7 Algarni H, Umar A, Kim S H, Al-Assiri M S & Alfaify S, *Nanosci Nanotechnol Lett*, 8 (2016) 521.
8 Maurer F, Dangwal A, Lysenkov D, Müller G, Toimil-Molares M E, Trautmann C, Brotz J & Fuess H, *Nucl Instrum Methods Phys Res B*, 245 (2006) 337.
9 Martin C R, *Chem Mater*, 8 (1996) 1739.
10 Toimil-Molares M E, Buschmann V, Dobrev D, Neumann R, Scholz R, Schuchert I U & Vetter J, *Adv Mater*, 13 (2001) 62.
11 Stepniowski W J, Moneta M, Karczewski K, Michalska-Domanska M, Czujko T, Mol J M C & Buijnsters J G, *J Electroanal Chem*, 809 (2018) 59.
12 Toimil-Molares M E, *Beilstein J Nanotechnol*, 3 (2012) 860.
13 Zhao S, Han F, Li J, Meng X, Huang W, Cao D, Zhang G, Sun R & Wong C P, *Small*, 14 (2018) 1800047.
14 Cao G & Liu D, *Adv Colloid Interface Sci*, 136 (2008) 45.
15 Inguanta R, Piazza S & Sunseri C, *Appl Surf Sci*, 255 (2009) 8816.
16 Narula C & Chauhan R P, *Phys: B Condensed Matter*, 521 (2017) 381.
17 Duan J L, Liu J, Yao H J, Mo D, Hou M D, Sun Y M, Chen Y F & Zhang L, *Mater Sci Eng B*, 147 (2008) 57.
18 Locharoenrat K, Sanoa H & Mizutani G, *Sci Technol Adv Mater*, 8 (2007) 277.
19 Qian X, Liu H, Guo Y, Song Y &Li Y, *Nanoscale Res Lett*, 3 (2008) 303.
20 Chakarvarti S K, *Radiat Meas*, 44 (2009) 1085.
21 Kumar N, Kumar R, Kumar S & Chakarvati S K, *Curr Appl Phys*, 14 (2014) 1547.
22 Nehra M, Dilbhagi A N, Singh V, Singhal N K & Kumar S, *Phys Status Solidi A*, 217 (2020) 190084.
23 Rana P, Narula C, Rani A, Chauhan R P, Gupta R & Kumar R, *J Mater Sci: Mater Electron*, 28 (2017) 9998.
24 Cho Y S & Huh Y D, *Mater Lett*, 63 (2009) 227.
25 Kumar N, Kumar R, Kumar S & Chakarvati S K, *Radiat Phys Chem*, 119 (2016) 44.
26 Cullity B D & Stock S R, Elements of X-ray diffraction (Pearson), 3rd Edn, 2001.
27 Williamson G K & Hall W H, *Acta Metall*, 1 (1953) 22.
28 Duan J L, Cornelius T W, Liu J, Karim S, Yao H J, Picht O, Rauber M, Muller S & Neumann R, *J Phys Chem C*, 113 (2009) 13583.
29 Gupta R, Chauhan R P, Chakarvarti S K, Jaiswal M K, Ghoshal D, Basu S, Suresh S, Bartolucci S F, Koratkar N & Kumar R, *J Mater Sci: Mater Electron*, 29 (2018) 190.
30 Feldman B, Park S, Haverty M, Shankar S &Dunham S T, *Phys Status Solidi B*, 247 (2010) 1791.
31 Henriqueza R, Flores M, Moraga L, Kremer G, Gonzalez-Fuentes C & Munoz R C, *Appl Surf Sci*, 273 (2013) 315.
32 Mayades A F & Shatzkes M, *Phys Rev B*, 1 (1970) 1382.
33 Fowler R H & Nordheim L, *Proc R Soc Lond*, 119 (1928) 1471.
34 Forbes R G & Deane B J H, *Proc R Soc A*, 463 (2007) 2907.
35 Kumar A, Parveen S, Husain S, Zulfiqar M, Harsh & Husain M, *J Alloys Compd*, 711 (2017) 85.